UC Berkeley

UC Berkeley Previously Published Works

Title

Single-cell multiome sequencing clarifies enteric glial diversity and identifies an intraganglionic population poised for neurogenesis

Permalink

https://escholarship.org/uc/item/2f28b1qn

Journal

Cell Reports, 42(3)

ISSN

2639-1856

Authors

Guyer, Richard A
Stavely, Rhian
Robertson, Keiramarie
et al.

Publication Date

2023-03-01

DOI

10.1016/j.celrep.2023.112194

Peer reviewed

eScholarship.org Powered by the California Digital Library
University of California

Author Manuscript

Author Manuscript

Author Manuscript

Author Manuscript

HHS Public Access

Author manuscript

Cell Rep. Author manuscript; available in PMC 2023 April 24.

Published in final edited form as:

Cell Rep. 2023 March 28; 42(3): 112194. doi:10.1016/j.celrep.2023.112194.

Single-cell multiome sequencing clarifies enteric glial diversity and identifies an intraganglionic population poised for neurogenesis

Richard A. Guyer[1], **Rhian Stavely**[1], **Keiramarie Robertson**[2,3], **Sukhada Bhave**[1], **Jessica L. Mueller**[1], **Nicole M. Picard**[1], **Ryo Hotta**[1], **Julia A. Kaltschmidt**[3,4], **Allan M. Goldstein**[1,5,*]

[1]Department of Pediatric Surgery, Massachusetts General Hospital, Boston, MA, USA

[2]Neurosciences Graduate Program, Stanford University, Stanford, CA, USA

[3]Wu Tsai Neurosciences Institute, Stanford University, Stanford, CA, USA

[4]Department of Neurosurgery, Stanford University School of Medicine, Stanford, CA, USA

[5]Lead contact

SUMMARY

The enteric nervous system (ENS) consists of glial cells (EGCs) and neurons derived from neural crest precursors. EGCs retain capacity for large-scale neurogenesis in culture, and *in vivo* lineage tracing has identified neurons derived from glial cells in response to inflammation. We thus hypothesize that EGCs possess a chromatin structure poised for neurogenesis. We use single-cell multiome sequencing to simultaneously assess transcription and chromatin accessibility in EGCs undergoing spontaneous neurogenesis in culture, as well as small intestine myenteric plexus EGCs. Cultured EGCs maintain open chromatin at genomic loci accessible in neurons, and neurogenesis from EGCs involves dynamic chromatin rearrangements with a net decrease in accessible chromatin. A subset of *in vivo* EGCs, highly enriched within the myenteric ganglia and that persist into adulthood, have a gene expression program and chromatin state consistent with neurogenic potential. These results clarify the mechanisms underlying EGC potential for neuronal fate transition.

Graphical abstract

This is an open access article under the CC BY-NC-ND license (http://creativecommons.org/licenses/by-nc-nd/4.0/).

*Correspondence: agoldstein@partners.org.

AUTHOR CONTRIBUTIONS

Conceptualization, R.A.G. and A.M.G.; methodology, R.A.G., A.M.G., K.R., J.A.K., and R.S.; formal analysis, R.A.G. and R.S.; investigation, R.A.G., S.B., K.R., J.L.M., and N.M.P.; resources, A.M.G., R.H., and J.A.K.; data curation, R.A.G. and R.S.; writing – original draft, R.A.G. and A.M.G.; writing – review & editing, R.A.G., R.S., K.R., J.A.K., R.H., N.M.P., J.L.M., and A.M.G.; supervision, A.M.G., R.H., and J.A.K.; project administration, A.M.G. and R.H.; funding acquisition, R.A.G., A.M.G., and J.A.K.

SUPPLEMENTAL INFORMATION

Supplemental information can be found online at https://doi.org/10.1016/j.celrep.2023.112194.

INCLUSION AND DIVERSITY

We support inclusive, diverse, and equitable conduct of research.

Author Manuscript
Author Manuscript
Author Manuscript
Author Manuscript

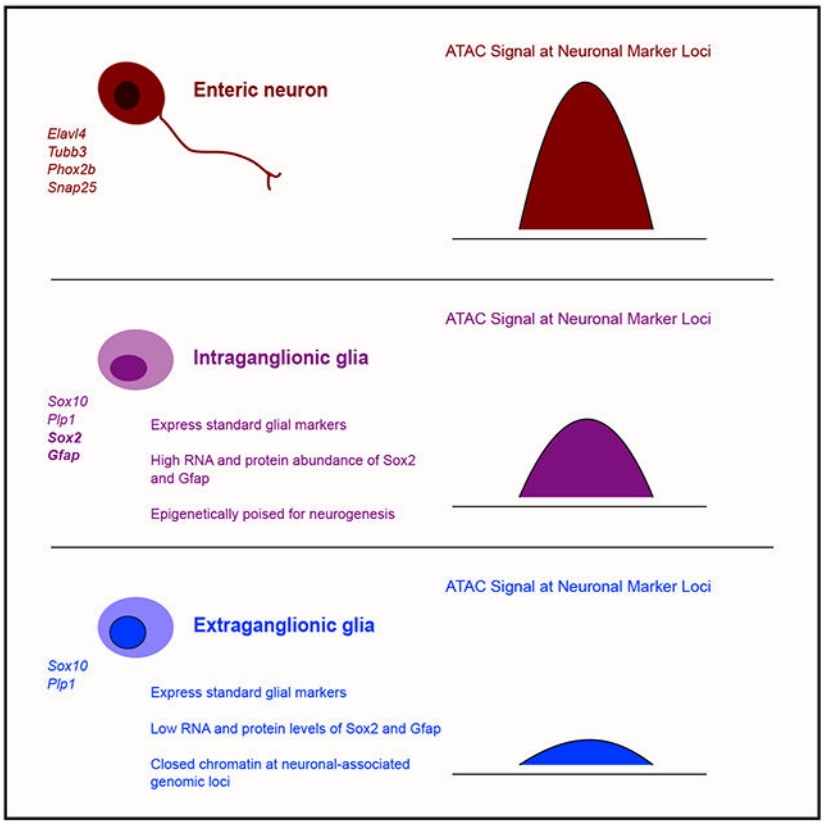

In brief

By performing comprehensive single-cell transcriptomic and chromatin accessibility profiling of enteric glial cells both in culture and freshly isolated from mouse small intestine, Guyer et al. identify intraganglionic glia as a distinct subpopulation of enteric glial cells that are epigenetically poised for neurogenesis.

INTRODUCTION

The enteric nervous system (ENS) controls gastrointestinal (GI) motility, secretion, absorption,[1] and immune regulation.[2] The ENS is composed of enteric glial cells (EGCs) and neurons derived from migrating enteric neural crest cells (ENCCs) during embryonic development.[3] Postnatal EGCs express many of the same markers as prenatal ENCCs, such as Sox10, p75, and Nestin,[4,5] and EGCs have been demonstrated to generate neurons both in culture and *in vivo* in response to injury.[4,6,7] These data suggest that EGCs maintain a multipotent state primed for neurogenesis.

Protein expression patterns of the glial markers proteolipid protein 1 (Plp1), Sox10, S100b, and glial fibrillary acidic protein (Gfap) suggest heterogeneity among EGCs,[8] but this has not been fully explored. Other evidence of functional diversity among EGCs include heterogeneous responses to purinergic stimulation, dye coupling of only a subset of glial cells within ganglia, and preferential stimulation of *Gfap* transcription in response to

Author Manuscript Author Manuscript Author Manuscript Author Manuscript

lipopolysaccharide exposure.[9–11] Several single-cell RNA sequencing (scRNA-seq) studies have captured EGCs and have reported multiple EGC clusters.[12,13] However, these studies did not report detailed analysis of EGC subtypes, nor did they assess differentiation of EGCs into neurons. Our current work extends these results by jointly assessing transcription and chromatin structure of EGCs both in their native environment and during *in vitro* neurogenesis.

The gene expression programs available to a cell are constrained by epigenetic factors including chromatin accessibility.[14] Open chromatin is sensitive to nuclease digestion and can be assessed by DNase I hypersensitivity or the assay for transposase-accessible chromatin (ATAC), the latter of which is a valuable tool for profiling chromatin in either bulk or single-cell samples.[15–17] While differentiation is a dynamic process involving both closing and opening of chromatin,[18] a net decrease in nuclease-sensitive regions characterizes greater restriction of cell fate potential.[19–21] Similarly, perturbations that prevent terminal differentiation are associated with increased chromatin accessibility.[22] Joint profiling of ATAC signal and gene expression can thus clarify how fate potential changes as cells adopt novel transcriptional programs.

We hypothesize that subpopulations of EGCs maintain a permissive chromatin structure for neuronal differentiation. In the present study, we apply scRNA-seq as well as multiome sequencing that simultaneously measure ATAC signal and RNA transcripts in individual nuclei (scMulti-seq) to characterize EGCs and study the dynamics of neuronal differentiation. We show that EGCs maintain open chromatin at promoters and regulatory elements controlling neuronal marker genes. Differentiation of EGCs into neurons involves reduced chromatin accessibility, consistent with more limited fate potential. scMulti-seq of EGCs freshly isolated from postnatal mouse intestine reveals considerable transcriptional diversity, consistent with previous reports.[13] By integrating gene expression with chromatin structure, we identify a subpopulation of EGCs primed for neurogenesis. *In situ* hybridization and immunofluorescence (IF) validate this population, demonstrate it to be heavily enriched within myenteric ganglia, and show that it persists beyond early postnatal life. Our work provides a multiomic atlas of myenteric EGCs, identifies a chromatin state poised for neurogenesis, and confirms intraganglionic EGCs to be biologically distinct from EGCs present in the extraganglionic environment.

RESULTS

EGCs spontaneously generate neurons in culture

We first sought to establish an *ex vivo* model for studying the EGC-to-neuron fate transition. We developed a dual-reporter system by crossing *Plp1::GFP* mice,[23] which mark all EGCs by GFP expression, with *Actl6b::Cre;(R)26-tdTomato* mice, which permanently mark cells committed to neuronal fate with tdTomato. We generated neurospheres using cells isolated from the longitudinal muscle-myenteric plexus (LMMP) layer of the small intestine of these dual-reporter mice (age 12–16 weeks) and then sorted GFP+/tdTomato− cells to obtain a pure EGC population. These EGCs were plated on fibronectin, and live-cell imaging was performed 1 and 5 days later. The day after plating, no tdTomato+ cells were seen, indicating that we successfully isolated a pure EGC population (Figure 1A). On day 5,

Author Manuscript Author Manuscript Author Manuscript Author Manuscript

however, a significant number of tdTomato+ neurons was noted, thus demonstrating that EGCs generate neurons in culture (Figure 1A). This confirms prior reports claiming that EGCs have neurogenic potential in culture.[4–7]

To determine whether active neurogenesis occurs within neurospheres, we sorted tdTomato− cells from the small intestine LMMP of *Actl6b::Cre;(R)26-tdTomato* mice (age 12–16 weeks) to obtain a population lacking committed neurons. We then generated neurospheres using this neuron-free population. After 7 days in neurosphere culture conditions, expression of tdTomato was apparent (Figure 1B), and flow cytometry analysis showed that approximately 4% of cells within the neurospheres were tdTomato+ committed neurons (Figure 1C), demonstrating active neurogenesis occurring within neurospheres.

To better understand neurogenesis within neurospheres, we performed scRNA-seq on both the GFP+ and GFP− cell fractions sorted from neurospheres that were grown for 10 days using LMMP cells from *Plp1::GFP* mice (age 12–16 weeks). Separate datasets obtained from male and female mice were integrated using the Seurat SCTransform workflow. The GFP− fraction was dominated by cells with a mesenchymal gene signature, which are known to promote ENS cell growth.[24] In contrast, the GFP+ fraction was heavily enriched for ENS marker genes (Figure S1A). As expected, the GFP− fraction included neurons (Figure S1B), which may represent either neurons present at the time of gut dissociation or newly generated neurons in which GFP protein has been degraded. The GFP+ fraction includes a large number of EGCs, as expected, but also proliferating cells, cells expressing genes characteristic of enteric neuroblasts,[25] and neurons (Figures 1D and 1F). The GFP+ fraction also includes a small number of cells with a mesenchymal gene expression pattern (Figure S1C). The neuroblasts and neuronal clusters contain progressively lower levels of Plp1 RNA (Figure 1F), and a cascade of gene expression changes from EGCs to neurons is evident (Figure 1E), which suggests neuronal differentiation from a glial cell of origin. The differentiation trajectory shows a similar pattern of gene expression changes as previously reported during embryonic ENS development in mice[25] (Figures 1F, S1D, and S1E), including the emergence of two distinct neuronal lineages marked, respectively, by *Bnc2* and *Etv1* transcripts (Figures 1D, 1F, S1D, and S1E). Based on these data, we conclude that EGCs isolated from adult mice can proliferate and that enteric neurosphere cultures are a useful model for studying enteric neurogenesis.

Multiome analysis of EGC-to-neuron transition within neurospheres reveals a chromatin structure poised for neurogenesis

To evaluate whether EGCs maintain chromatin permissive for neurogenesis, we performed scMulti-seq to simultaneously obtain gene expression and ATAC data on GFP+ cells within neurospheres grown from *Plp1::GFP* mice. These data represent cells from three mice cultured together. Dimensional reduction and clustering were performed using ATAC data, and cell identities were confirmed based on gene expression. This approach revealed a similar hierarchy as seen in our scRNA-seq data, with a large population of EGCs, two clusters of neurons, an intervening population of neuroblasts, and a cluster of proliferating cells (Figures 2A and 2B). To further confirm the validity of clustering via ATAC data, we used ChromVAR[26] to identify transcription factor binding motif enrichments. Consistent

Author Manuscript Author Manuscript Author Manuscript Author Manuscript

with a fate transition from glial cells to neurons, we found a switch from SOX10 and SOX2 motif enrichment to ASCL1 and PHOX2B motif enrichment (Figures 2C and S2A). As expected during differentiation from a multipotent progenitor to a more differentiated state, we observed a net closing of chromatin during the transition from EGCs to neurons (Figures 2D and 2E). The chromatin changes during the EGC-to-neuron transition are dynamic, with many EGC-associated ATAC peaks showing diminished signal in cell populations further along the differentiation vector. Conversely, chromatin becomes increasingly accessible at peaks associated with neuronal cells (Figure 2F). For example, several peaks around the Sox10 gene show markedly diminished signal as cells progress toward a neuronal fate (Figure 2H). Interestingly, many ATAC peaks that are associated with neuroblasts or neurons are nuclease sensitive in EGCs (Figures 2F, 2G, and 2I), suggesting that they are regulatory elements that can be activated to trigger neurogenesis. We examined an ATAC peak within a non-coding region of the *Camta1* gene, which is associated with neuronal differentiation,[27] and saw that while the chromatin accessibility is greatest in neuroblasts, glial cells are also nuclease sensitive in this region (Figure 2I).

We identified 578 genes whose RNA expression marks neuroblasts and neurons in our dataset. When individual cells were scored for a gene expression program defined by these genes, marked enrichment was seen in the neuroblast and neuron clusters (Figure S2B). We then identified ATAC peaks that are positively or negatively correlated with expression of these genes and examined the ATAC signal within the coding regions of these genes, as well as within 2,000 base pairs (bps) of the upstream promoter and 1,000 bps downstream from the end of the coding region. To our surprise, the majority of upstream promoter regions for these 578 neuroblast- and neuron-associated genes were accessible in EGCs and displayed only a small increase in signal during neuronal differentiation (Figures S2C and S2D). This is illustrated by the neuronal marker gene *Tubb3*, which has similar accessibility around the transcriptional start site (TSS) in EGCs, neuroblasts, and neurons (Figure S2E). The 578 genes were positively linked with 1,634 ATAC peaks and negatively linked with 385 peaks. In contrast to signal in their promoter regions, there was a marked shift in signal at the linked peaks (Figures S2B and S2C), with dramatic shifts in nuclease sensitivity along the trajectory of neurogenesis. We conclude that the promoter regions of neuronal lineage-defining genes are primed for rapid induction in EGCs and that such induction occurs when regulatory elements are activated or repressed.

EGCs in the postnatal small intestine are transcriptionally diverse and include cells with a chromatin structure primed for neurogenesis

Although neurospheres derived from LMMP cells can model enteric neurogenesis, cultures may not reflect the biology of EGCs *in vivo*. We thus undertook scRNA-seq and scMulti-seq of GFP+ cells freshly isolated from the small intestine LMMP of *Plp1::GFP* mice at or near postnatal day 14 (P14). We integrated these datasets using the Seurat SCTransform workflow[28,29] and performed dimensional reduction and clustering based on the expression of highly variable genes. We filtered out low-quality cells and manually removed small numbers of cells that co-expressed markers of both glial cells (*Sox10, Plp1*) and either neurons (*Tubb3, Uchl1*) or smooth muscle cells (*Acta2*). Although prior literature has suggested that EGCs can generate both neurons and myofibroblasts,[4,13] we could not rule

Author Manuscript Author Manuscript Author Manuscript Author Manuscript

out the possibility of doublet contamination, so these cells were excluded from further analysis. We were left with 17,690 EGCs, 3,754 of which had both gene expression and ATAC data, characterized by 9 transcriptionally distinct clusters (Figures 3A and S3A). We observed two clusters of proliferating cells marked by cell-cycle-associated genes (*Mki67, Cenpf, Hells, Pcna*). Interestingly, we noted an inverse correlation between expression of several glial markers, including *Plp1, Sox10, Sox6*, and *Itga2* (which were high in clusters 0, 2, 3, 7, and 8) and *Gfap, S100b*, and *Sox2* (high in clusters 1 and 4; Figure 3B). Cluster 4 was marked by high expression of *Slc18a2, Ramp1*, and *Cpe* (Figure 2B), the first of which was previously identified as a marker of a subset of EGCs in mouse colon.[12] While the levels were low, a small number of cells in cluster 1 also expressed these same transcripts (Figure 2B). Clusters 1 and 4 were relatively enriched for genes encoding transcription factors associated with neuronal differentiation, including *Phox2b, Hand2, Tbx3, Ascl1, Hoxa5*, and *Hoxb5* (Figure 3B). We also found that genes previously identified as EGC markers in bulk RNA-seq studies, such as *Kcna1* and *Col20a1*,[8] had low expression in cluster 4 relative to other EGCs (Figure 3B). These data show that postnatal EGCs are a heterogeneous population that includes a subset (clusters 1 and 4) expressing genes associated with neurogenesis. While these two clusters are relatively small, together they account for 20.9% of cells (Figure 3C).

For further confirmation that cluster 4 contains EGCs poised for neurogenesis, we again used ChromVAR. Among the motifs enriched in cluster 4, we noted PHOX2B, PHOX2A, and HAND2 (Figure 3D), all of which are factors associated with neuronal differentiation.[25] We examined the ATAC signal at the 1,588 neuroblast marker peaks identified in our neurosphere model (Figure 2F). We saw that the ATAC signal was enriched at neuroblast peaks in cluster 4 and, to a lesser degree, in cluster 1 (Figure 3E). A volcano plot of the 457 neuroblast peaks with ATAC counts >0 in both cluster 4 cells and all other cells shows clear skewing of individual neuroblast-associated peaks toward enrichment in cluster 4 (Figure 3F).

We next examined global chromatin accessibility. We found most glial clusters to display a similar degree of chromatin accessibility, with some diminished signal in proliferating cells. The notable exception was cluster 8, which had a significantly lower ATAC signal at most peaks (Figure 3G). We also noted that cluster 8 showed the strongest inverse correlation with cluster 4 regarding neuroblast peak signal (Figure 3E). We assessed ATAC signal in the promoter and coding regions of the 578 neuronal marker genes previously identified in our neurosphere model (Figures S2B). As in the neurospheres, most EGCs *in vivo* maintain accessible chromatin upstream of these genes' TSS. Cluster 8 was again noted to be an exception, with significantly diminished signal relative to other clusters (Figure 3G). This is illustrated by the neuronal marker *Elavl4*, which is nuclease sensitive around its TSS in all clusters except cluster 8 (Figure 3H). These results indicate that EGCs in the postnatal mouse intestine contain a subpopulation primed for neurogenesis (clusters 1 and 4), as well as another subpopulation (cluster 8) with a restricted chromatin structure and decreased chromatin accessibility near the TSS of neuronal marker genes. Cluster 8 was distinguished from other glial clusters by high transcription of several non-coding RNAs (Figure S3A), such as *Gm42418* and *Gm26917*. While the significance of these non-coding transcripts is unclear, they are reported to correlate with important biological functions in

Author Manuscript Author Manuscript Author Manuscript Author Manuscript

other cell types.[30–32] Cells with this transcriptional signature were identified in all four samples (Figure S3B and S3C), and standard quality metrics for scATAC-seq data were comparable for cluster 8 as for other clusters (Figure S3D). While we did not investigate cluster 8 further, it may be a subset of postnatal EGCs lacking neurogenic potential.

In vivo EGCs are similar to EGCs in neurosphere culture

To assess whether *ex vivo* culture produces cells that are comparable to *in vivo* EGCs, we used the Seurat SCTransform workflow to integrate our scRNA-seq datasets derived from either neurospheres or *in vivo* EGCs. Dimensional reduction and clustering showed that the cells grouped closely together, suggesting similarity (Figures S4A and S4B). Most clusters included cells from both groups, although clusters 7 and 10, which represent neuroblasts and neurons from neurospheres, contained virtually no *in vivo* EGCs (Figures S4C and S4D). Cluster 3, which is enriched for transcripts encoding adhesion molecules and matrix proteins (Figure S4D), is drawn almost exclusively from *in vivo* EGCs, and clusters 2 and 12, which are enriched for the same genes, predominantly include *in vivo* EGCs (Figure S4C). Interestingly, neurosphere cells are enriched for *Cpe* and *Gfap* RNAs, for transcripts encoding the neuroblast transcription factors *Ascl1* and *Sox11*, and for the neuronal marker transcript *Tubb3* (Figure S4E). Conversely, *in vivo* ECGs express higher levels of the glia-defining factors *Sox10* and *Sox6* than cells in neurospheres (Figure S4E). These data indicate that neurosphere cultures predominantly contain EGCs poised for neurogenesis, while *in vivo* EGCs also include cells with roles in establishing and interacting with the extracellular environment.

EGCs with neurogenic potential are restricted to myenteric ganglia in mice before and after weaning

Having identified a gene expression signature associated with neuronal precursor status in EGCs, we next performed IF to validate this population *in vivo*. LMMP from the small intestine of *Plp1::GFP* mice was used for this analysis. Because Gfap protein expression has been reported to mark a subset of EGCs,[8] we first evaluated Gfap protein expression. We found that GFP+ EGCs within myenteric ganglia express Gfap at much higher levels than extraganglionic EGCs in both P14 mice and adult animals at 14 weeks age (Figures 4A and 4B), both recapitulating prior reports[8] and suggesting that this population is not transient early in life. Our single-cell data suggest that *Sox2*, which denotes neuronal stem cells and is critical for their maintenance,[33,34] is expressed in a similar population as *Gfap* (Figure 3B). To confirm this, we similarly performed IF on LMMP from P14 mice and mice aged 14 weeks. Gfap and Sox2 proteins were heavily enriched in the myenteric ganglia of mice at both ages (Figures 4C and 4D). Because EGCs mice aged 12–16 weeks proliferate in neurosphere culture (Figure 1B), we also suspected that EGCs retain proliferative capability beyond the early postnatal period. We thus pulsed both P14 and 14-week-old *Plp1::GFP* mice with EdU for 7 days, followed by LMMP harvest and confocal imaging. Unsurprisingly, mice in the early postnatal period display significant proliferation of EGCs (Figure 4F). Older mice also exhibit EdU staining in rare EGCs within myenteric ganglia (Figures 4E and 4F), demonstrating that these cells do not lose the ability to proliferate after weaning.

Author Manuscript Author Manuscript Author Manuscript Author Manuscript

As further validation, we undertook RNAscope[35] imaging of LMMP tissue from P14 and 10.5-week-old *Plp1::GFP* mice (Figure S5A). Consistent with the scRNA-seq data, *Gfap* was detected in only a subset of EGCs (Figures 4G–4I and S5B), although the proportion of EGCs with *Gfap* transcripts detected was considerably higher by *in situ* hybridization, possibly reflecting greater sensitivity of RNAscope for detection of genes with low transcript abundance. We observed that *Gfap* transcripts are considerably enriched within the myenteric ganglia compared with extraganglionic EGCs (Figures 4G–4I, S5B, and S5C). This persists after weaning, although total Gfap transcript abundance does decline (Figure S5B). Transcripts of four other genes that are co-enriched with *Gfap* in cluster 1 (Figure 3A) were also evaluated (*Sox2, Cpe, Ramp1*, and *Slc18a2*). In each case, enrichment of these transcripts within myenteric ganglia was apparent (Figures 4G–4I and S5C). Quantification showed that cells dual positive for *Gfap* transcripts and each of these four transcripts represented a large majority of cells within the myenteric ganglia (Figures 4G–4I). Transcripts of *Slc18a2* were particularly scarce outside of the ganglia (Figures 4H and S5C). When we compare P14 mice and postweaning animals, this pattern persists (Figures 4G–4I and S5C), with all statistically significant differences between age groups accounted for by diminished *Gfap* transcript abundance. Taken together, our IF and RNAscope results validate the presence of an EGC subpopulation marked by co-expression of *Gfap, Sox2, Cpe, Ramp1*, and *Slc18a2* transcripts, which represents cells apparently poised for neurogenesis and demonstrates that these cells are heavily enriched within myenteric ganglia. Moreover, this population persists beyond the early postnatal period.

DISCUSSION

Postnatal EGCs are a heterogeneous population of cells[8,13] possessing the capacity to generate neurons both in culture and *in vivo* in response to injury.[4–7] Our present work, which leverages scMulti-seq technology to examine cultured and *in vivo* EGCs, confirms that EGCs are progenitors of enteric neurons, identifies intraganglionc glial cells as having a transcriptional and epigenetic state poised for neurogenesis, and identifies a chromatin state in EGCs that is likely to maintain multipotency. In addition, we demonstrate that neurogenesis in neurosphere culture closely recapitulates the transcriptional events observed during embryonic enteric neuronal development.[25] This finding, combined with the fact that neurospheres are an easily accessible experimental model and can be generated in large numbers from a single mouse intestine, establishes them as a reliable system for studying the molecular mechanisms of enteric neurogenesis. The similarity between glial-derived neurogenesis in neurosphere cultures and embryonic neurogenesis further suggests that large-scale expansion of EGCs as neurospheres *in vitro* may be a valuable source of enteric neuronal progenitors for cell therapy applications.[36]

By utilizing scMulti-seq, we have clarified the molecular basis underlying the neuronal potential of EGCs. We find EGCs to have a more open chromatin structure than enteric neurons, which is a hallmark of cells at earlier points along a differentiation vector.[19–21] As EGCs become neurons, their chromatin changes dynamically, with closing of EGC-associated sites and opening at neuronal-associated loci both occurring. EGCs, both in culture and in their native environment, maintain open chromatin at loci that characterize neuroblasts. These accessible chromatin sites likely include regulatory elements that can

Author Manuscript Author Manuscript Author Manuscript Author Manuscript

be activated to initiate a cascade of transcriptional and epigenetic changes culminating in neuronal commitment. Such a process has been demonstrated in the mouse hair follicle, where increased ATAC signal at enhancers and promoters precedes changes in gene expression that determine cell fate.[37] Further characterization of this process will require profiling DNA modifications, histone marks, and transcription factor binding during neurogenesis, which will undoubtedly be facilitated by the emergence of tools for measuring such parameters in individual cells.[38–40]

Interestingly, we found that EGCs both in culture and in the small intestine maintain open chromatin around the transcription start sites of many neuronal marker genes despite low expression of these genes. An ATAC signal is generally correlated with gene expression,[14] although cells can maintain accessible chromatin within the promoters of genes that are not actively transcribed,[41] and an ATAC signal within promoters is a sign of impending transcription during development.[37] A high ATAC signal within the promoter regions of neuronal marker genes suggests that EGCs are poised for neurogenesis. We speculate that EGCs repress neuronal lineage-determining genes via mechanisms other than chromatin accessibility to prevent inappropriate neurogenesis and that such repression is relieved upon receipt of differentiation signals. Given these observations, EGCs may display bivalent chromatin within promoters of neuronal lineage-determining genes, which would allow for their rapid activation,[42] but this remains to be determined. We also identified a group of EGCs marked by expression of non-coding RNAs and more restricted chromatin structure. While the biological significance of this population is uncertain, we speculate it may represent EGCs without neuronal potential.

We used both IF and RNAscope to validate the transcriptional heterogeneity we identified among myenteric EGCs both early in life and weeks after weaning. RNAscope identified *Gfap* transcripts in a considerably higher proportion of EGCs than scRNA-seq, a discrepancy we suspect is due to greater sensitivity of the RNAscope assay, although inefficient isolation of single cells from ganglia may also contribute. Nevertheless, the results confirm that *Gfap* transcription correlates with *Sox2, Cpe, Ramp1*, and *Slc18a2. Slc18a2* has previously been identified as an EGC cluster marker in the mouse colon and small intestine,[12,13] which demonstrates scRNA-seq to be a reproducible tool for identifying EGC populations. *Gfap*-expressing EGCs also express RNAs that encode transcription factors associated with neurogenesis (such as *Phox2b, Phox2a, Ascl1*, and *Hoxa5*), have a higher signal at neuroblast-associated ATAC peaks than other EGC clusters, and are enriched for neuronal transcription factor binding motifs. Based on these data, we believe *Gfap*-expressing EGCs represent the glial cells that are poised for neurogenesis. IF and RNAscope revealed that the *Gfap*-expressing EGCs are heavily enriched within the myenteric ganglia. This recapitulates the results of Rao et al.,[8] who found via immunostaining that Gfap protein is largely confined to ganglia. We speculate that spatial restriction reflects different functions for intra- and extraganglionic EGCs. Intraganglionic EGCs likely include a reservoir of potential neurons, while the greater expression of extracellular matrix genes, such as *Col20a1*, and ion channel genes, such as *Kcna1*, in extraganglionic EGCs probably reflect other functions important for intestinal homeostasis.

Author Manuscript Author Manuscript Author Manuscript Author Manuscript

An important question raised by this study is what factors maintain intraganglionic EGCs in a state poised for neurogenesis. Neurogenesis from EGCs in mature mice has been observed after inflammatory insults or chemical ablation of neurons.[5–7] One possibility, which has yet to be tested, is that signals to EGCs from neurons restrain differentiation and that relief of such signals results in neurogenesis. If this is the case, it is possible that intraganglionic EGCs are simply ENCCs whose progression toward neuronal fate was interrupted when neuronal density in their proximity reached a threshold level. Careful lineage tracing coupled with assessment of transcriptional and epigenetic changes during pre- and postnatal ENS development would be necessary to evaluate this intriguing hypothesis. Another critical question is whether postnatal EGCs can generate all subtypes of enteric neurons. Under neurosphere culture conditions, they do give rise to neurons from both of the main lineage branches identified recently,[25] but further experimentation will be needed to assess this *in vivo*.

In summary, this study provides a multiome atlas of mouse EGCs and provides a valuable, publicly available resource for the scientific community. By integrating gene expression and ATAC data at the single-cell level, we have found that the transition from EGC fate to neuronal fate involves dynamic epigenome rearrangements. A subset of EGCs that is heavily enriched within the myenteric ganglia appear poised for neurogenesis. These cells persist and retain proliferative capability beyond the early postnatal period. Our data will inform studies to identify the critical signaling networks and transcriptional circuitries underlying the EGC's decision to either remain multipotent or become a neuron.

Limitations of the study

scMulti-seq was performed only on EGCs from pups around P14. While we did validate persistence of an intraganglionic population marked by *Gfap/Sox2/Slc18a2/Cpe/Ramp1* transcripts and Gfap and Sox2 proteins after weaning, our study does not address chromatin changes after maturation. Our study is limited to EGCs from the LMMP, so neither submucosal EGCs nor Schwann cells accompanying extrinsic nerve fibers are included. Extrinsic Schwann cells have been suggested as a source of myenteric neurons in adult animals and may have similar epigenetic potential.[43] Our data reflect a pooled population of EGCs from the entire small intestine, so neither gastric nor colonic cells are included. Regional variation in chromatin state or gene expression along the small intestine, as previously reported,[8,12] may be masked in our data. Although ATAC data allow for inference of regulatory elements and transcription factor binding patterns,[44,45] profiling of histone modifications and transcription factor binding can add additional information but is outside the scope of this resource. Finally, as is the current standard, we have used enzymatic digestion and cell sorting to isolate EGCs from the LMMP layer. This cell isolation technique has been shown to activate artifactual gene signatures in diverse tissues, including brain microglia[46,47]; scMulti-seq including ATAC may mitigate this problem, as the ATAC signal delineates cell identity more robustly than RNA.[48]

Author Manuscript Author Manuscript Author Manuscript Author Manuscript

STAR★METHODS

RESOURCE AVAILABILITY

Lead contact—Further information and requests for resources and reagents should be directed to and will be fulfilled by the lead contact, Allan M. Goldstein (agoldstein@partners.org).

Materials availability—This study did not generate new unique reagents.

Data and code availability

- Single-cell RNA sequencing data and single-cell ATAC sequencing data have been deposited at GEO and are publicly available as of the date of publication. Accession numbers are listed in the key resources table. Original microscopy images have been deposited at Mendeley and are publicly available as of the date of publication. The DOIs are listed in the key resources table.
- This paper does not report original code.
- Any additional information required to reanalyze the data reported in this paper is available from the lead contact upon request.

EXPERIMENTAL MODEL AND SUBJECT DETAILS

Ethical statement—This study was performed according to experimental protocols approved by the Institutional Animal Care and Use Committees of Massachusetts General Hospital and Stanford University.

Animals—*Plp1::GFP* mice were gifted to the Goldstein laboratory by Wendy Macklin[23] or purchased from Jackson Laboratories (Bar Harbor, ME) (stock number 033357). Animals homozygous for GFP expression were used for scRNA-seq, while animals heterozygous for GFP expression were used for RNAscope studies. Both homozygous and heterozygous animals were used for immunoflouresence studies. *Actl6b::Cre* (stock number 027826) and *(R)26-tdTomato* (stock number 007914) mice were purchased from Jackson Laboratories.[52,53] Dual reporter mice were generated by first crossing *Actl6b::Cre* animals with *(R)26-tdTomato* animals, and subsequently crossing offspring with *Plp1::GFP* animals to yield *Plp1::GFPI/ Actl6b::Cre;(R)26-tdTomato* offspring.

Primary cultures—*Plp1::GFP* mice aged 12-16 weeks were euthanized and their small intestine was removed from duodenum to terminal ileum. The longitudinal muscle-myenteric plexus (LMMP) layer, which contains myenteric ganglia, was carefully dissected from underlying tissue under a dissecting microscope in ice-cold PBS supplemented with 10% bovine serum albumin. After dissection, LMMP tissue was digested for 60 minutes at 37° C in dispase (250 μg/ml; STEMCELL Technologies, Vancouver, BC) and collagenase XI (1mg/ml; Sigma-Aldrich, St. Louis, MO). Following digestion, the cells were filtered via a 40 micron filter to ensure a single-cell suspension. Immediately after digestion and filtering, cells were counted and resuspended at a density of 10^5 cells/mL in a 1:1 mixture of DMEM (Thermo Fisher, Waltham, MA) and NeuroCult Basal Media (STEMCELL

Author Manuscript Author Manuscript Author Manuscript Author Manuscript

Technologies, Vancouver, BC) supplemented with 20 ng/mL FGF, 20 ng/mL IGF1, 2% B27 supplement, 1% N2 supplement, 50 mM b-mercaptoethanol, and 75 ng/mL retinoic acid. 10^5 cells/mL in a total volume of 10 mL were placed 10cm flasks (Corning Inc, Corning, NY) at 37° C and 5% CO_2 for 7-10 days. Media was replaced on day 5 by centrifuging cells at 250g for 3 minutes followed by re-suspension in fresh media and return to the same flasks and incubator for 5 more days. Cells from both male and female mice were used and were cultured separately.

METHOD DETAILS

Cell sorting—Cell sorting was performed by the Harvard Stem Cell Institute's Center for Regenerative Medicine Flow Cytometry Core facility located on the Massachusetts General Hospital campus. Sorting was performed on BD Bioscences (Franklin Lakes, NJ) FACSAria sorting instruments.

Preparation of scRNA-seq libraries—For postnatal mice, LMMP cells were isolated from *Plp1::GFP* mice and sorted for GFP+ cells as described above. Immediately after sorting, cells were manually counted with Trypan blue to assess viability. Cells were then delivered immediately to the MGH NextGen Sequencing Core Facility and core staff prepared cDNA libraries using the 10X Genetics v3.0 kits. The standard 10X Genetics workflow was used. Cells from 4 mice were used in three batches, with the first batch containing pooled cells from 1 male and 1 female mouse and the remaining two batches each containing cells from a single mouse (1 male, 1 female). Each batch was run on a separate GEM chip lane. For scRNA-seq of three-dimensional (3D) cultures, single cells were obtained by digesting cultures for 45 minutes with Accutase (STEMCELL Technologies, Vancouver, BC). Cells were then sorted as described above into GFP+ and GFP− populations and immediately returned to the laboratory where they were manually counted with Trypan blue to assess viability. After determining viable cell counts, a 10X Chromium Controller located in our facility was used along with 10X Genetics (Pleasanton, CA) v3.1 kits to generate gel bead emulsions (GEMs), followed by library preparation according to the manufacturer's protocol. Cells from 4 mice were used to generate 3D cultures for scRNA-seq, with cells from 2 male mice and 2 female mice each pooled together and cultured separately. Cells from cultures of male and female mice were run on separate GEM chip lanes.

Preparation of multiomic libraries—For adolescent mice, LMMP was isolated from P16-18 animals as described above and GFP+ cells were sorted. Cells from three male mice were pooled and run on one lane of a GEM chip. 10X Genetics Multiomic kits were used, and GEMs were generated using the 10X Chromium Controller located in our facility. snATAC libraries were generated using the standard 10X Genetics workflow. For multiomic analysis of neurosphere cultures, LMMP cells from three 12-week-old *Plp1::GFP* mice were pool and grown in suspension culture conditions for 10 days. Cells were then dissociated and sorted to isolate the GFP+ population. A single lane on a GEM chip was then used to generate GEMs. The 10X Genetics multiomic library preparation workflow was undertaken in accordance with the manufacturer's protocol.

Author Manuscript Author Manuscript Author Manuscript Author Manuscript

Sequencing and genome alignment—All sequencing was performed at the Harvard University Bauer Core Facility, where libraries were sequenced on either Illumina NextSeq or Illumina NovaSeq instruments. Demultiplexing, genome alignment, and feature-barcode matrix generation was performed with the 10X Genetics Cell Ranger software pipeline.[49]

Single cell data analysis—scRNA-seq and snMulti-seq data was analyzed with the open-source Seurat and Signac packages implemented in the R computing environment. For the postnatal glial scRNA-seq dataset and neurosphere datasets, cells more than one standard deviation away from the mean number of genes detected were filtered, as were cells with greater than 10% mitochondrial genes. Datasets were integrated using the SCTransform workflow in Seurat.[28] After integration, principle component analysis (PCA) was performed. Neighbors were identified and UMAP projection was performed using the first 30 principal components. Clusters were identified using the "FindClusters" command with resolution = 0.5 using the Louvain algorithm.[54] Where indicated, data were manually annotated based on expression of known marker genes.

ATAC data was processed using the standard Signac workflow. Briefly, cells with fewer than 1000 or more than 100,000 ATAC fragments were filtered, as were cells with nucleosomal enrichment > 2 or transcriptional start site enrichment < 1. Peaks within each dataset were identified using MACS2.[50] Dimensional reduction was performed with latent semantic indexing (LSI) via the "RunTFIDF" command, "FindTopFeatures" function with min.cutoff set to 5, and "RunSVD" function. UMAP projection was performed utilizing LSI components 2-50.

Transcription factor motif enrichement was implemented with the ChromVAR software package implemented through Signac.[26] JASPAR 2020 vertebrate transcription factor motifs were utilized.[55] ChromVAR results were imported to Signac as an assay object. To identify a gene set characteristic of neuroblasts and neurons, gene markers for each clusters were identified using the Seurat "FindAllMakers" command with the following settings: min.pct = 0.25, test.use = "wilcox", only.pos = TRUE, logfc.threshold = 0.25. Unique marker genes of the clusters "Neuroblast," "Neuron1," and "Neuron2" were then selected and filtered to include only those with an adjusted p value < 0.0001 and a log2-fold change > 0.5 relative to other clusters. ATAC peaks linked with gene expression were calculated by using the Signac "LinkPeaks" command with default settings. Peak sets and gene loci were exported in BED format.[56]

ATAC data visualization—BAM files for each cluster were generated using Sinto (https://timoast.github.io/sinto/). Cluster BAM files were used to generate bigWig files using the deepTools[51] bamCoverage function with RPGC normalization, binSize =10, smoothLength = 50, effectiveGenomeSize = 2652783500, and extendReads = 150. deepTools computeMatrix was then used with the scaling indicated for each figure, and plots were generated using deepTools plotHeatmap or plotProfile. For heatmaps, zMin was set to 0 and zMax was set to the 90th percentile value for the cluster with the highest median expression, as determined by using the deepTools computeMatrixOperations dataRange command. Tracks plots were generated using the Integrative Genomics Viewer v2.11.1.[57]

Author Manuscript Author Manuscript Author Manuscript Author Manuscript

Live cell imaging—GFP+/tdTomato− cells were sorted from LMMP suspension cultures derived from *Plp1::GFP/ Actl6b::Cre;(R)26-tdTomato* dual reporter mice. Cells were placed in adherent culture conditions in neuronal differentiation media, which consists of BrainPhys Neuronal Media (STEMCELL Technologies, Vancouver, BC) supplemented with 1% N2 supplement and 2% NeuroCult S1 supplement (STEMCELL Technologies, Vancouver, BC). After one day media was removed and replaced with a thin layer of phosphate buffered saline. Cells were then imaged at 10x magnification using a Keyence microscope. After imaging, differentiation media was replaced and cells were returned to culture for 4 more days. Repeat imaging was performed in the same manner after 5 days in culture.

Immunoflouresence imaging—LMMP preparations from either P14 or 14 week-old *Plp1::GFP* mice were fixed for 4-6 hours in 4% paraformaldehyde. Tissues were blocked in PBS supplemented with 10% donkey serum, 10% bovine serum albumin, and 1% triton in PBS for 1 hour at room temperature. LMMP preparations were then incubated at 4°C overnight in primary antibodies, which were diluted in the blocking solution. Primary antibodies included goat anti-GFAP (1:500; Abcam ab53554) and goat anti-Sox2 (1:50; R&D Systems AF2018). Tissues were then incubated for 3 hours at room temperature in secondary antibodies, which were also diluted in blocking buffer. The secondary antibody used was donkey anti-goat IgG (1:500; Alexa Fluor 546; Invitrogen A-11056). Cell nuclei were stained with DAPI (Invitrogen D1306) and tissues were mounted with aqua-poly/ mount (Polysciences Inc 18606-20). Images were acquired at 1024 × 1024 pixels using a 20X air immersion objective on a ZEISS Laser Confocal Scanning Microscope 800 with Airyscan.

EdU proliferation assay—P14 and 14 week-old mice were injected intraperitoneally with EdU (Invitrogen, A10044) at a dose of 50 mg/kg for 5 days. On day 5, the mice were sacrificed 1 hour post-injection and LMMP was harvested. LMMP preparations were fixed for 4-6 hours in 4% paraformaldehyde. Click-iT EdU Cell Proliferation Kit for Imaging (Fisher Scientific, C10340) was used per the manufacturer's protocol. Cell nuclei were stained with DAPI (Invitrogen D1306) and tissues were mounted with aqua-poly/mount (Polysciences Inc 18606-20). Images were acquired at 1024 × 1024 pixels using a 20X air immersion objective on a ZEISS Laser Confocal Scanning Microscope 800 with Airyscan.

RNAScope—Mice were euthanized and their small intestine was removed from the duodenum to the ileum. The small intestine was cut into three segments and each segment was cut along the mesentery. The cut segments were laid flat on filter paper and fixed for 24 hours in 4% PFA. Under a dissecting microscope, the LMMP was carefully peeled away from the lamina propria. Protein-RNA co-detection was performed using RNA-protein Co-detection ancillary kit (ACD, 323180) according to manufactures instructions with adaptions for LMMP sections. Briefly, LMMP sections were post fixed in 4% paraformaldehyde for 15 minutes in a 12-well plate. Tissue was transferred into staining nets and dehydrated by a serial ethanol gradient (50%, 70%, 100%, 100%) for 5 minutes each. Tissue was then placed into a 96-well plate and incubated in hydrogen peroxide for 15 minutes. Tissue was briefly rinsed in water and incubated in codetect target antigen retrieval solution for 5 minutes in a steamer. Tissue was rinsed in water and incubated overnight with anti-GFP antibody

Author Manuscript Author Manuscript Author Manuscript Author Manuscript

(Abcam, ab13970) diluted 1:250 in co-detection diluent. RNAscope was performed using RNAscope multiplex fluorescent reagent kit V2 (ACD, 323100). All RNAscope incubation and washes were performed in 80-well microtitration trays (International Scientific Supplies, WHO080). Tissue was washed in 0.2% PBT and post-fixed in 10% NBF for 30 minutes at room temperature. Tissue was digested with Protease Plus for 25 minutes at 40°C. Tissue was incubated for 2 hours in RNAscope probes for *Gfap* (313211-C3), *Sox2* (401041-C2), *Slc18a2* (425331), *Ramp1* (532681-C2) or *Cpe* (454091). Negative and positive control probes were used to confirm specificity of probes and presence of background noise. Amplification and probe development steps were performed according to manufacture instruction. Tissue was incubated for 30 minutes in Alexa Flour 647 Goat anti-chicken secondary antibody (Invitrogen, A21449) diluted at 1:250 in co-diluent. Tissue was then mounted on slides and cover slipped for imaging. A Leica SP8 confocal microscope was used to acquire large tile images. Tiles were stitched together using the Navigation mode in the LAS X software. Z-stacks with 2μm between each focal plane were acquired for 25-35μm thick sections. A 20x oil objective was used to acquire all images.

Quantification of RNAscope labeling was performed with ImageJ v1.53c using methods previously described for the measurement of fluorescence in confocal images.[58] Glial cells were identified by *Plp1* promoter-driven expression of GFP in Z-stack projections. Binary thresholding was performed on GFP expression using the default ImageJ algorithm. Glial cell bodies were identified using the “analyze particles” feature for objects over 20μm^2. Individual GFP-expressing glia were manually annotated based on intra- or extraganglionic location, and 100 intraganglionic and 100 extraganglionic cells were arbitrarily selected from each sample for further analysis. ROIs generated from the particle analysis of individual glia were used to measure the background corrected mean fluorescence intensity (MFI)[59] for RNAscope probes in each cell. Cells with a MFI >1 were considered to be positively labeled for calculating the proportion of cells expressing each marker. This process is illustrated in Figure S5A.

Published scRNA-seq data—Data of the mouse embryonic ENS at P15.5 and P185 was published previously.[25] This data was obtained from the NCBI Sequence Read Archive. Runs SRR11635571, SRR11635572, and SRR11635573 were downloaded using the SRA Toolkit “fastq-dump” command. Genome alignment and feature-barcode matrix generation was performed with the Cell Ranger “cellranger count” command on the Mass General Brigham ERISOne Research Computing Cluster. Further analysis was performed with Seurat in the R environment. Briefly, the datasets were filtered as the authors describe in the original paper, with removal of cells with < 1000 genes detected, > 6000 genes detected, > 40,000 total RNA counts, and > 5% mitochondrial genes detected. Datasets were then integrated using the standard Seurat workflow. Following integration, PCA was performed and UMAP projection was undertaken with the top 30 principle components.

QUANTIFICATION AND STATISTICAL ANALYSIS

Statistical analysis was performed in GraphPad Prism 9.4.1. All graphs display data as mean, with error bars representing standard deviation unless noted otherwise in the figure legend. Details of statistical analysis specified in the results section and in the figure legends.

Author Manuscript Author Manuscript Author Manuscript Author Manuscript

Supplementary Material

Refer to Web version on PubMed Central for supplementary material.

ACKNOWLEDGMENTS

The authors are grateful for the expertise offered by the Harvard University Bauer Core and the Harvard Stem Cell Institute Center for Regenerative Medicine Flow Cytometry Core facility. This work was supported by the National Institute of Diabetes and Digestive and Kidney Diseases (grants F32DK121440 to R.A.G. and R01DK119210 to A.M.G.), by the Department of Neurosurgery of Stanford University School of Medicine (J.A.K.), and by the Firmenich Next Generation Fund (J.A.K.). K.R.'s work was supported by National Institutes of Health training grant T32MH020016 awarded to Stanford University School of Medicine.

DECLARATION OF INTERESTS

A.M.G. receives research funds from Takeda Pharmaceutical Company.

REFERENCES

1. Furness JB (2012). The enteric nervous system and neurogastroenterology. Nat. Rev. Gastroenterol. Hepatol 9, 286–294. 10.1038/nrgastro.2012.32. [PubMed: 22392290]
2. Jacobson A, Yang D, Vella M, and Chiu IM (2021). The intestinal neuro-immune axis: crosstalk between neurons, immune cells, and microbes. Mucosal Immunol 14, 555–565. 10.1038/s41385-020-00368-1. [PubMed: 33542493]
3. Nagy N, and Goldstein AM (2017). Enteric nervous system development: a crest cell's journey from neural tube to colon. Semin. Cell Dev. Biol 66, 94–106. 10.1016/j.semcdb.2017.01.006. [PubMed: 28087321]
4. Joseph NM, He S, Quintana E, Kim Y-G, Núñez G, and Morrison SJ (2011). Enteric glia are multipotent in culture but primarily form glia in the adult rodent gut. J. Clin. Invest 121, 3398–3411. 10.1172/JCI58186. [PubMed: 21865643]
5. Laranjeira C, Sandgren K, Kessaris N, Richardson W, Potocnik A, Vanden Berghe P, and Pachnis V (2011). Glial cells in the mouse enteric nervous system can undergo neurogenesis in response to injury. J. Clin. Invest 121, 3412–3424. 10.1172/JCI58200. [PubMed: 21865647]
6. Belkind-Gerson J, Hotta R, Nagy N, Thomas AR, Graham H, Cheng L, Solorzano J, Nguyen D, Kamionek M, Dietrich J, et al. (2015). Colitis induces enteric neurogenesis through a 5-HT4–dependent mechanism. Inflamm. Bowel Dis 21, 870–878. 10.1097/MIB.0000000000000326. [PubMed: 25742399]
7. Belkind-Gerson J, Graham HK, Reynolds J, Hotta R, Nagy N, Cheng L, Kamionek M, Shi HN, Aherne CM, and Goldstein AM (2017). Colitis promotes neuronal differentiation of Sox2+ and PLP1+ enteric cells. Sci. Rep 7, 2525. 10.1038/s41598-017-02890-y. [PubMed: 28566702]
8. Rao M, Nelms BD, Dong L, Salinas-Rios V, Rutlin M, Gershon MD, and Corfas G (2015). Enteric glia express proteolipid protein 1 and are a transcriptionally unique population of glia in the mammalian nervous system. Glia 63, 2040–2057. 10.1002/glia.22876. [PubMed: 26119414]
9. Boesmans W, Lasrado R, Vanden Berghe P, and Pachnis V (2015). Heterogeneity and phenotypic plasticity of glial cells in the mammalian enteric nervous system. Glia 63, 229–241. 10.1002/glia.22746. [PubMed: 25161129]
10. Maudlej N, and Hanani M (1992). Modulation of dye coupling among glial cells in the myenteric and submucosal plexuses of the Guinea pig. Brain Res 578, 94–98. 10.1016/0006-8993(92)90234-Z. [PubMed: 1380866]
11. Rosenbaum C, Schick MA, Wollborn J, Heider A, Scholz C-J, Cecil A, Niesler B, Hirrlinger J, Walles H, and Metzger M (2016). Activation of myenteric glia during acute inflammation in vitro and in vivo. PLoS One 11, e0151335. 10.1371/journal.pone.0151335. [PubMed: 26964064]
12. Drokhlyansky E, Smillie CS, Van Wittenberghe N, Ericsson M, Griffin GK, Eraslan G, Dionne D, Cuoco MS, Goder-Reiser MN, Sharova T, et al. (2020). The human and mouse enteric nervous

Author Manuscript Author Manuscript Author Manuscript Author Manuscript

system at single-cell resolution. Cell 182, 1606–1622.e23. 10.1016/j.cell.2020.08.003. [PubMed: 32888429]

13. Zeisel A, Hochgerner H, Lönnerberg P, Johnsson A, Memic F, van der Zwan J, Häring M, Braun E, Borm LE, La Manno G, et al. (2018). Molecular architecture of the mouse nervous system. Cell 174, 999–1014.e22. 10.1016/j.cell.2018.06.021. [PubMed: 30096314]
14. Wu J, Huang B, Chen H, Yin Q, Liu Y, Xiang Y, Zhang B, Liu B, Wang Q, Xia W, et al. (2016). The landscape of accessible chromatin in mammalian preimplantation embryos. Nature 534, 652–657. 10.1038/nature18606. [PubMed: 27309802]
15. Boyle AP, Davis S, Shulha HP, Meltzer P, Margulies EH, Weng Z, Furey TS, and Crawford GE (2008). High-resolution mapping and characterization of open chromatin across the genome. Cell 132, 311–322. 10.1016/j.cell.2007.12.014. [PubMed: 18243105]
16. Buenrostro JD, Giresi PG, Zaba LC, Chang HY, and Greenleaf WJ (2013). Transposition of native chromatin for fast and sensitive epigenomic profiling of open chromatin, DNA-binding proteins and nucleosome position. Nat. Methods 10, 1213–1218. 10.1038/nmeth.2688. [PubMed: 24097267]
17. Satpathy AT, Granja JM, Yost KE, Qi Y, Meschi F, McDermott GP, Olsen BN, Mumbach MR, Pierce SE, Corces MR, et al. (2019). Massively parallel single-cell chromatin landscapes of human immune cell development and intratumoral T cell exhaustion. Nat. Biotechnol 37, 925–936. 10.1038/s41587-019-0206-z. [PubMed: 31375813]
18. Jadhav U, Saxena M, O'Neill NK, Saadatpour A, Yuan G-C, Herbert Z, Murata K, and Shivdasani RA (2017). Dynamic reorganization of chromatin accessibility signatures during dedifferentiation of secretory precursors into Lgr5+ intestinal stem cells. Cell Stem Cell 21, 65–77.e5. 10.1016/j.stem.2017.05.001. [PubMed: 28648363]
19. Baumann C, Zhang X, Zhu L, Fan Y, and De La Fuente R (2021). Changes in chromatin accessibility landscape and histone H3 core acetylation during valproic acid-induced differentiation of embryonic stem cells. Epigenet. Chromatin 14, 58. 10.1186/s13072-021-00432-5.
20. Stergachis AB, Neph S, Reynolds A, Humbert R, Miller B, Paige SL, Vernot B, Cheng JB, Thurman RE, Sandstrom R, et al. (2013). Developmental fate and cellular maturity encoded in human regulatory DNA landscapes. Cell 154, 888–903. 10.1016/j.cell.2013.07.020. [PubMed: 23953118]
21. Ugarte F, Sousae R, Cinquin B, Martin EW, Krietsch J, Sanchez G, Inman M, Tsang H, Warr M, Passegué E, et al. (2015). Progressive chromatin condensation and H3K9 methylation regulate the differentiation of embryonic and hematopoietic stem cells. Stem Cell Rep 5, 728–740. 10.1016/j.stemcr.2015.09.009.
22. Wenderski W, Wang L, Krokhotin A, Walsh JJ, Li H, Shoji H, Ghosh S, George RD, Miller EL, Elias L, et al. (2020). Loss of the neural-specific BAF subunit ACTL6B relieves repression of early response genes and causes recessive autism. Proc. Natl. Acad. Sci. USA 117, 10055–10066. 10.1073/pnas.1908238117. [PubMed: 32312822]
23. Mallon BS, Shick HE, Kidd GJ, and Macklin WB (2002). Proteolipid promoter activity distinguishes two populations of NG2-positive cells throughout neonatal cortical development. J. Neurosci 22, 876–885. [PubMed: 11826117]
24. Stavely R, Bhave S, Ho WLN, Ahmed M, Pan W, Rahman AA, Ulloa J, Bousquet N, Omer M, Guyer R, et al. (2021). Enteric mesenchymal cells support the growth of postnatal enteric neural stem cells. Stem Cell. 39, 1236–1252. 10.1002/stem.3388.
25. Morarach K, Mikhailova A, Knoflach V, Memic F, Kumar R, Li W, Ernfors P, and Marklund U (2021). Diversification of molecularly defined myenteric neuron classes revealed by single-cell RNA sequencing. Nat. Neurosci 24, 34–46. 10.1038/s41593-020-00736-x. [PubMed: 33288908]
26. Schep AN, Wu B, Buenrostro JD, and Greenleaf WJ (2017). chrom-VAR: inferring transcription-factor-associated accessibility from single-cell epigenomic data. Nat. Methods 14, 975–978. 10.1038/nmeth.4401. [PubMed: 28825706]
27. Henrich K-O, Bauer T, Schulte J, Ehemann V, Deubzer H, Gogolin S, Muth D, Fischer M, Benner A, König R, et al. (2011). CAMTA1, a 1p36 tumor suppressor candidate, inhibits growth and activates differentiation programs in neuroblastoma cells. Cancer Res 71, 3142–3151. 10.1158/0008-5472.CAN-10-3014. [PubMed: 21385898]

Author Manuscript Author Manuscript Author Manuscript Author Manuscript

28. Hafemeister C, and Satija R (2019). Normalization and variance stabilization of single-cell RNA-seq data using regularized negative binomial regression. Genome Biol 20, 296. 10.1186/s13059-019-1874-1. [PubMed: 31870423]
29. Choudhary S, and Satija R (2022). Comparison and evaluation of statistical error models for scRNA-seq. Genome Biol 23, 27. 10.1186/s13059-021-02584-9. [PubMed: 35042561]
30. Chen Z, Bu N, Qiao X, Zuo Z, Shu Y, Liu Z, Qian Z, Chen J, and Hou Y (2018). Forkhead box M1 transcriptionally regulates the expression of long noncoding RNAs Snhg8 and Gm26917 to promote proliferation and survival of muscle satellite cells. Stem Cell. 36, 1097–1108. 10.1002/stem.2824.
31. Zhao D, Guo J, Liu L, and Huang Y (2021). Rosiglitazone attenuates high glucose-induced proliferation, inflammation, oxidative stress and extracellular matrix accumulation in mouse mesangial cells through the Gm26917/miR-185-5p pathway. Endocr. J 68, 751–762. 10.1507/endocrj.EJ20-0783. [PubMed: 33790061]
32. Zhang P, Cao L, Zhou R, Yang X, and Wu M (2019). The lncRNA Neat1 promotes activation of inflammasomes in macrophages. Nat. Commun 10, 1495. 10.1038/s41467-019-09482-6. [PubMed: 30940803]
33. Pagin M, Pernebrink M, Giubbolini S, Barone C, Sambruni G, Zhu Y, Chiara M, Ottolenghi S, Pavesi G, Wei C-L, et al. (2021). Sox2 controls neural stem cell self-renewal through a Fos-centered gene regulatory network. Stem Cell. 39, 1107–1119. 10.1002/stem.3373.
34. Amador-Arjona A, Cimadamore F, Huang C-T, Wright R, Lewis S, Gage FH, and Terskikh AV (2015). SOX2 primes the epigenetic landscape in neural precursors enabling proper gene activation during hippocampal neurogenesis. Proc. Natl. Acad. Sci. USA 112, E1936–E1945. 10.1073/pnas.1421480112. [PubMed: 25825708]
35. Wang F, Flanagan J, Su N, Wang L-C, Bui S, Nielson A, Wu X, Vo H-T, Ma X-J, and Luo Y (2012). RNAscope: a novel in situ RNA analysis platform for formalin-fixed, paraffin-embedded tissues. J. Mol. Diagn 14, 22–29. 10.1016/j.jmoldx.2011.08.002. [PubMed: 22166544]
36. Burns AJ, Goldstein AM, Newgreen DF, Stamp L, Schäfer KH, Metzger M, Hotta R, Young HM, Andrews PW, Thapar N, et al. (2016). White paper on guidelines concerning enteric nervous system stem cell therapy for enteric neuropathies. Dev. Biol 417, 229–251. 10.1016/j.ydbio.2016.04.001. [PubMed: 27059883]
37. Ma S, Zhang B, LaFave LM, Earl AS, Chiang Z, Hu Y, Ding J, Brack A, Kartha VK, Tay T, et al. (2020). Chromatin potential identified by shared single-cell profiling of RNA and chromatin. Cell 183, 1103–1116.e20. 10.1016/j.cell.2020.09.056. [PubMed: 33098772]
38. Ahn J, Heo S, Lee J, and Bang D (2021). Introduction to single-cell DNA methylation profiling methods. Biomolecules 11, 1013. 10.3390/biom11071013. [PubMed: 34356635]
39. Bartosovic M, Kabbe M, and Castelo-Branco G (2021). Single-cell CUT&Tag profiles histone modifications and transcription factors in complex tissues. Nat. Biotechnol 39, 825–835. 10.1038/s41587-021-00869-9. [PubMed: 33846645]
40. Kaya-Okur HS, Wu SJ, Codomo CA, Pledger ES, Bryson TD, Henikoff JG, Ahmad K, and Henikoff S (2019). CUT&Tag for efficient epigenomic profiling of small samples and single cells. Nat. Commun 10, 1930. 10.1038/s41467-019-09982-5. [PubMed: 31036827]
41. Starks RR, Biswas A, Jain A, and Tuteja G (2019). Combined analysis of dissimilar promoter accessibility and gene expression profiles identifies tissue-specific genes and actively repressed networks. Epigenet. Chromatin 12, 16. 10.1186/s13072-019-0260-2.
42. Bernstein BE, Mikkelsen TS, Xie X, Kamal M, Huebert DJ, Cuff J, Fry B, Meissner A, Wernig M, Plath K, et al. (2006). A bivalent chromatin structure marks key developmental genes in embryonic stem cells. Cell 125, 315–326. 10.1016/j.cell.2006.02.041. [PubMed: 16630819]
43. Uesaka T, Nagashimada M, and Enomoto H (2015). Neuronal differentiation in Schwann cell lineage underlies postnatal neurogenesis in the enteric nervous system. J. Neurosci 35, 9879–9888. 10.1523/JNEUROSCI.1239-15.2015. [PubMed: 26156989]
44. Akerberg BN, Gu F, VanDusen NJ, Zhang X, Dong R, Li K, Zhang B, Zhou B, Sethi I, Ma Q, et al. (2019). A reference map of murine cardiac transcription factor chromatin occupancy identifies dynamic and conserved enhancers. Nat. Commun 10, 4907. 10.1038/s41467-019-12812-3. [PubMed: 31659164]

Author Manuscript Author Manuscript Author Manuscript Author Manuscript

45. Galang G, Mandla R, Ruan H, Jung C, Sinha T, Stone NR, Wu RS, Mannion BJ, Allu PKR, Chang K, et al. (2020). ATAC-seq reveals an Isl1 enhancer that regulates sinoatrial node development and function. Circ. Res 127, 1502–1518. 10.1161/CIRCRESAHA.120.317145. [PubMed: 33044128]
46. Adam M, Potter AS, and Potter SS (2017). Psychrophilic proteases dramatically reduce single-cell RNA-seq artifacts: a molecular atlas of kidney development. Development 144, 3625–3632. 10.1242/dev.151142. [PubMed: 28851704]
47. Marsh SE, Walker AJ, Kamath T, Dissing-Olesen L, Hammond TR, de Soysa TY, Young AMH, Murphy S, Abdulraouf A, Nadaf N, et al. (2022). Dissection of artifactual and confounding glial signatures by single-cell sequencing of mouse and human brain. Nat. Neurosci 25, 306–316. 10.1038/s41593-022-01022-8. [PubMed: 35260865]
48. Corces MR, Buenrostro JD, Wu B, Greenside PG, Chan SM, Koenig JL, Snyder MP, Pritchard JK, Kundaje A, Greenleaf WJ, et al. (2016). Lineage-specific and single-cell chromatin accessibility charts human hematopoiesis and leukemia evolution. Nat. Genet 48, 1193–1203. 10.1038/ng.3646. [PubMed: 27526324]
49. Zheng GXY, Terry JM, Belgrader P, Ryvkin P, Bent ZW, Wilson R, Ziraldo SB, Wheeler TD, McDermott GP, Zhu J, et al. (2017). Massively parallel digital transcriptional profiling of single cells. Nat. Commun 8, 14049. 10.1038/ncomms14049. [PubMed: 28091601]
50. Zhang Y, Liu T, Meyer CA, Eeckhoute J, Johnson DS, Bernstein BE, Nusbaum C, Myers RM, Brown M, Li W, et al. (2008). Model-based analysis of ChIP-seq (MACS). Genome Biol 9, R137. 10.1186/gb-2008-9-9-r137. [PubMed: 18798982]
51. Ramírez F, Dündar F, Diehl S, Grüning BA, and Manke T (2014). deepTools: a flexible platform for exploring deep-sequencing data. Nucleic Acids Res 42, W187–W191. 10.1093/nar/gku365. [PubMed: 24799436]
52. Madisen L, Zwingman TA, Sunkin SM, Oh SW, Zariwala HA, Gu H, Ng LL, Palmiter RD, Hawrylycz MJ, Jones AR, et al. (2010). A robust and high-throughput Cre reporting and characterization system for the whole mouse brain. Nat. Neurosci 13, 133–140. 10.1038/nn.2467. [PubMed: 20023653]
53. Zou M, Luo H, and Xiang M (2015). Selective neuronal lineages derived from Dll4-expressing progenitors/precursors in the retina and spinal cord. Dev. Dyn 244, 86–97. 10.1002/dvdy.24185. [PubMed: 25179941]
54. Blondel VD, Guillaume J-L, Lambiotte R, and Lefebvre E (2008). Fast unfolding of communities in large networks. J. Stat. Mech 2008, P10008. 10.1088/1742-5468/2008/10/P10008.
55. Fornes O, Castro-Mondragon JA, Khan A, van der Lee R, Zhang X, Richmond PA, Modi BP, Correard S, Gheorghe M, Baranašić D, et al. (2020). JASPAR 2020: update of the open-access database of transcription factor binding profiles. Nucleic Acids Res 48, D87–D92. 10.1093/nar/gkz1001. [PubMed: 31701148]
56. Kent WJ, Sugnet CW, Furey TS, Roskin KM, Pringle TH, Zahler AM, and Haussler D (2002). The human genome browser at UCSC. Genome Res 12, 996–1006. 10.1101/gr.229102. [PubMed: 12045153]
57. Robinson JT, Thorvaldsdóttir H, Winckler W, Guttman M, Lander ES, Getz G, and Mesirov JP (2011). Integrative genomics viewer. Nat. Biotechnol 29, 24–26. 10.1038/nbt.1754. [PubMed: 21221095]
58. Schindelin J, Arganda-Carreras I, Frise E, Kaynig V, Longair M, Pietzsch T, Preibisch S, Rueden C, Saalfeld S, Schmid B, et al. (2012). Fiji: an open-source platform for biological-image analysis. Nat. Methods 9, 676–682. 10.1038/nmeth.2019. [PubMed: 22743772]
59. Shihan MH, Novo SG, Le Marchand SJ, Wang Y, and Duncan MK (2021). A simple method for quantitating confocal fluorescent images. Biochem. Biophys. Rep 25, 100916. 10.1016/j.bbrep.2021.100916. [PubMed: 33553685]

Author Manuscript Author Manuscript Author Manuscript Author Manuscript

Highlights

- Single-cell RNA and chromatin accessibility profiling of enteric glial cells
- Enteric glial cells undergo dynamic chromatin remodeling during neurogenesis
- Intraganglionic enteric glial cells have distinct RNA and ATAC profiles
- Intraganglionic enteric glia maintain chromatin poised for neurogenesis

Author Manuscript Author Manuscript Author Manuscript Author Manuscript

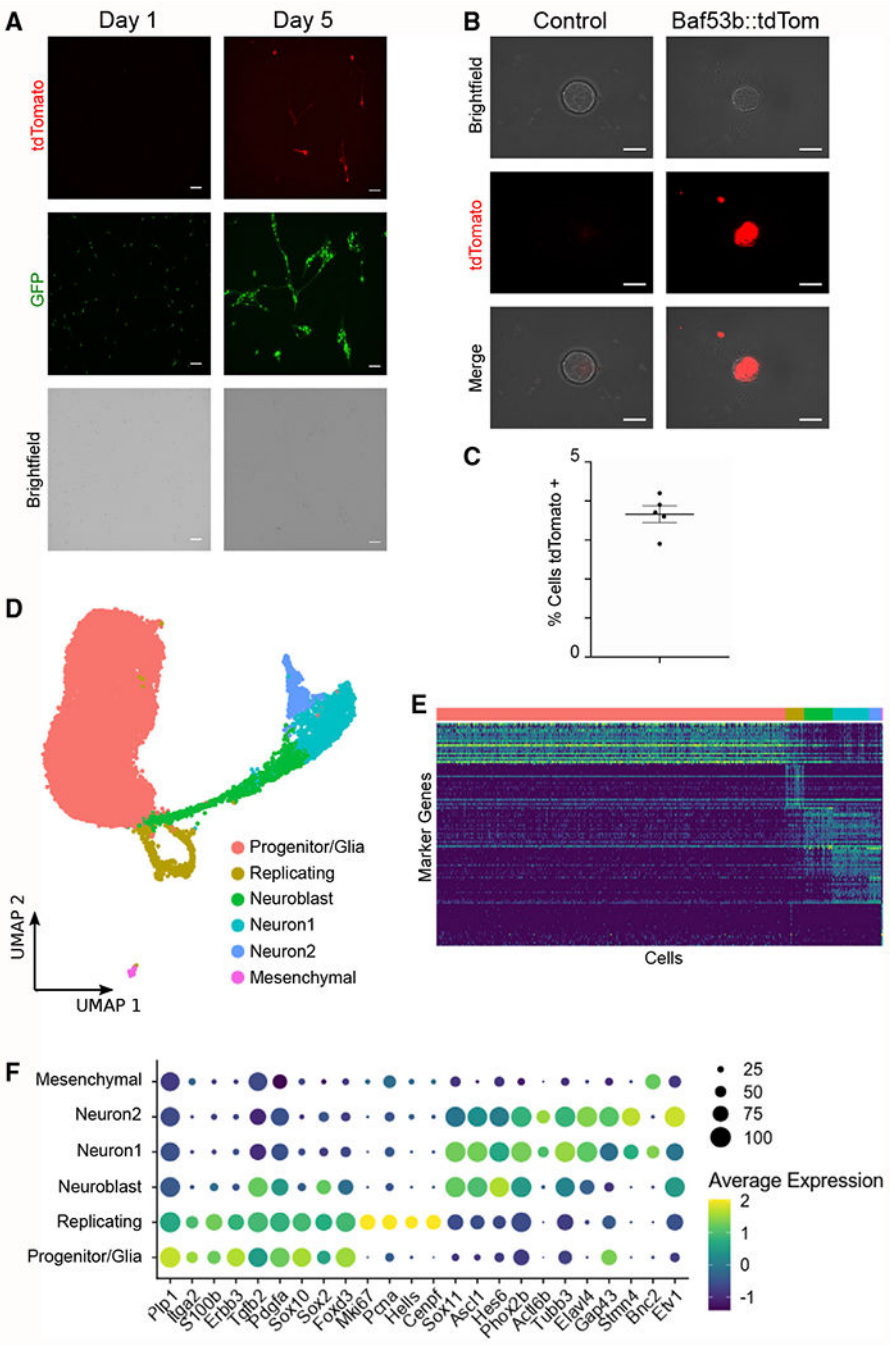

Figure 1. EGCs are neuronal progenitors in culture

(A) GFP+/tdTomato (tdT)− enteric glial cells isolated from *Plp1::GFP/Baf53b::Cre;R26tdT* dual-reporter mice give rise to tdT+ neurons in culture. Images are representative of results obtained from two biological replicates. Scale bars indicate 100 μm.

(B) tdT− cells sorted from the small intestine of *Baf53b::Cre;R26tdT* mice generate tdT+ cells when grown as neurospheres. Images are representative examples obtained using cells isolated from one control mouse and one *Baf53b::Cre;R26tdT* mouse. Scale bars indicate 100 μm.

Author Manuscript Author Manuscript Author Manuscript Author Manuscript

(C) Flow cytometry quantification of tdT+ cells in neurospheres grown using tdT− cells sorted from the small intestine of *Baf53b::Cre;R26tdT* mice. Error bars represent standard error of the mean. n = 5 biological replicates, with each replicate representing neurospheres grown with cells isolated from a separate mouse.
(D) Uniform manifold approximation and projection (UMAP) of 15,426 GFP+ cells sorted from neurospheres grown from the LMMP cells of *Plp1::GFP* mice, with major cell types highlighted, demonstrates a continuum of gene expression patterns from glial cells to neurons.
(E) Single-cell heatmap with cells grouped by cluster, showing the top 25 marker genes for each cluster based on fold change in expression relative to other clusters.
(F) Dot plot showing expression of selected marker genes for each cluster. Dot size indicates the percentage of cells in each cluster with >0 transcripts detected, while color indicates the relative level of gene expression.

Author Manuscript Author Manuscript Author Manuscript Author Manuscript

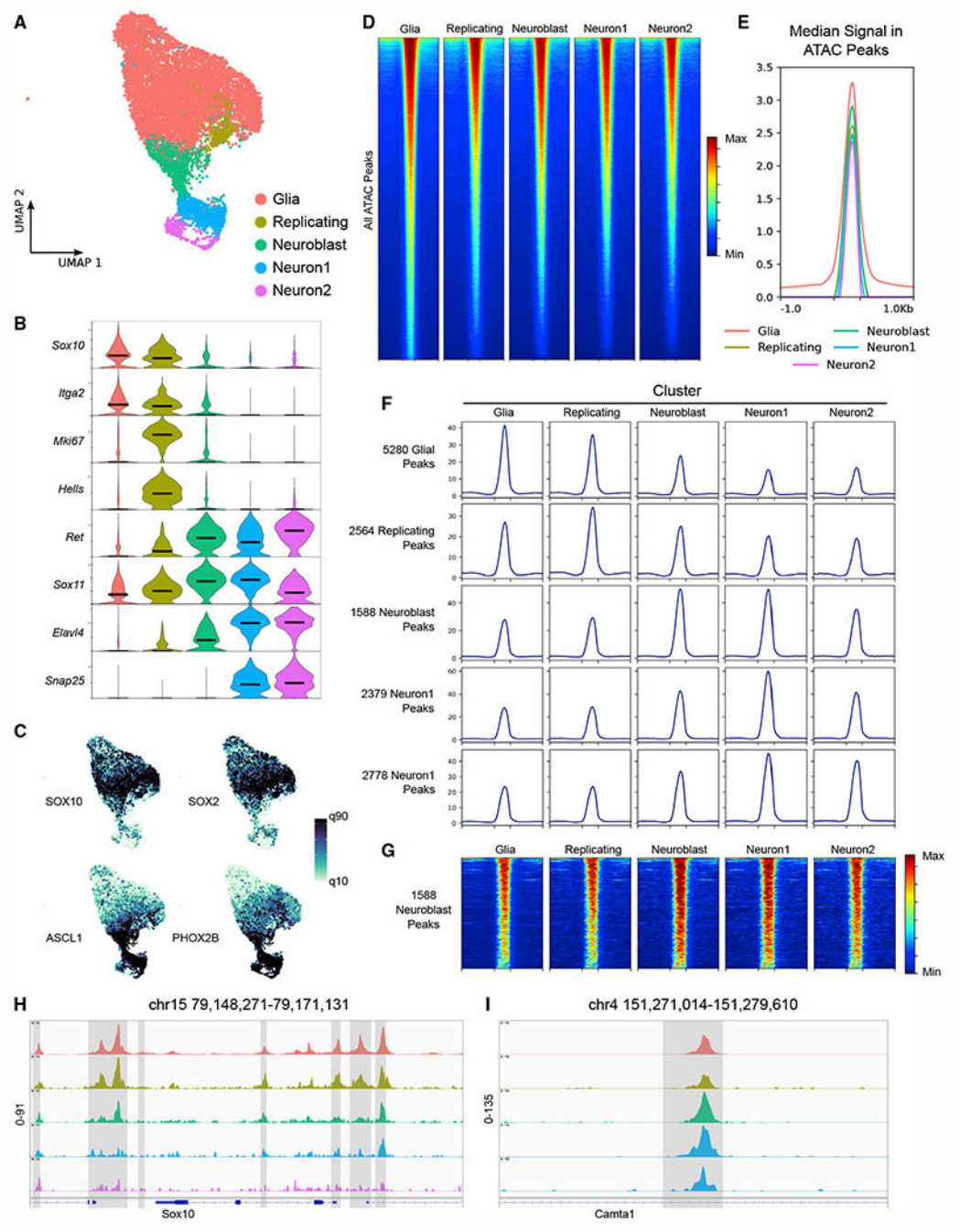

Figure 2. Multiome sequencing reveals chromatin poised for neurogenesis in EGCs in neurospheres

(A) UMAP of 10,328 GFP+ cells sorted from neurospheres grown from the LMMP of *Plp1::GFP* mice, with dimensional reduction performed based on ATAC signal. Major cell types are highlighted.

(B) Violin plot showing expression of selected marker genes in each major cell type. Dark bars indicate median expression.

(C) UMAPs colored based on enrichment for the indicated transcription factor binding motifs, with cutoffs at the 10^{th} and 90^{th} quantiles.

Author Manuscript Author Manuscript Author Manuscript Author Manuscript

(D) Heatmaps showing signal within each cluster at all 171,799 ATAC peaks identified in the dataset by MACS2. Peaks are scaled to 500 bps, and 1,000 bps up- and downstream are shown.

(E) Profile plot showing the median signal at each position within all 171,799 ATAC peaks. Peaks are scaled as in (D).

(F) Profile plots showing average signal intensity within each cluster at the indicated set of peaks. Peaks are scaled as in (D).

(G) Heatmaps showing signal at the indicated 1,587 neuroblast peaks within each cluster. Peaks are scaled as in (D).

(H) IGV Browser track showing ATAC signal within each cluster in the region around the *Sox10* gene locus. Peaks identified by the MACS2 algorithm are highlighted in gray.

(I) IGV Browser track showing ATAC signal within each cluster in the region around an ATAC peak within a non-coding region of the *Camta1* gene that marks neuroblasts. The peak region as identified by the MACS2 algorithm is highlighted in gray. The highest peaks are seen in the neuroblast and neuron1 clusters, but a signal is also apparent in the glia cluster.

Author Manuscript Author Manuscript Author Manuscript Author Manuscript

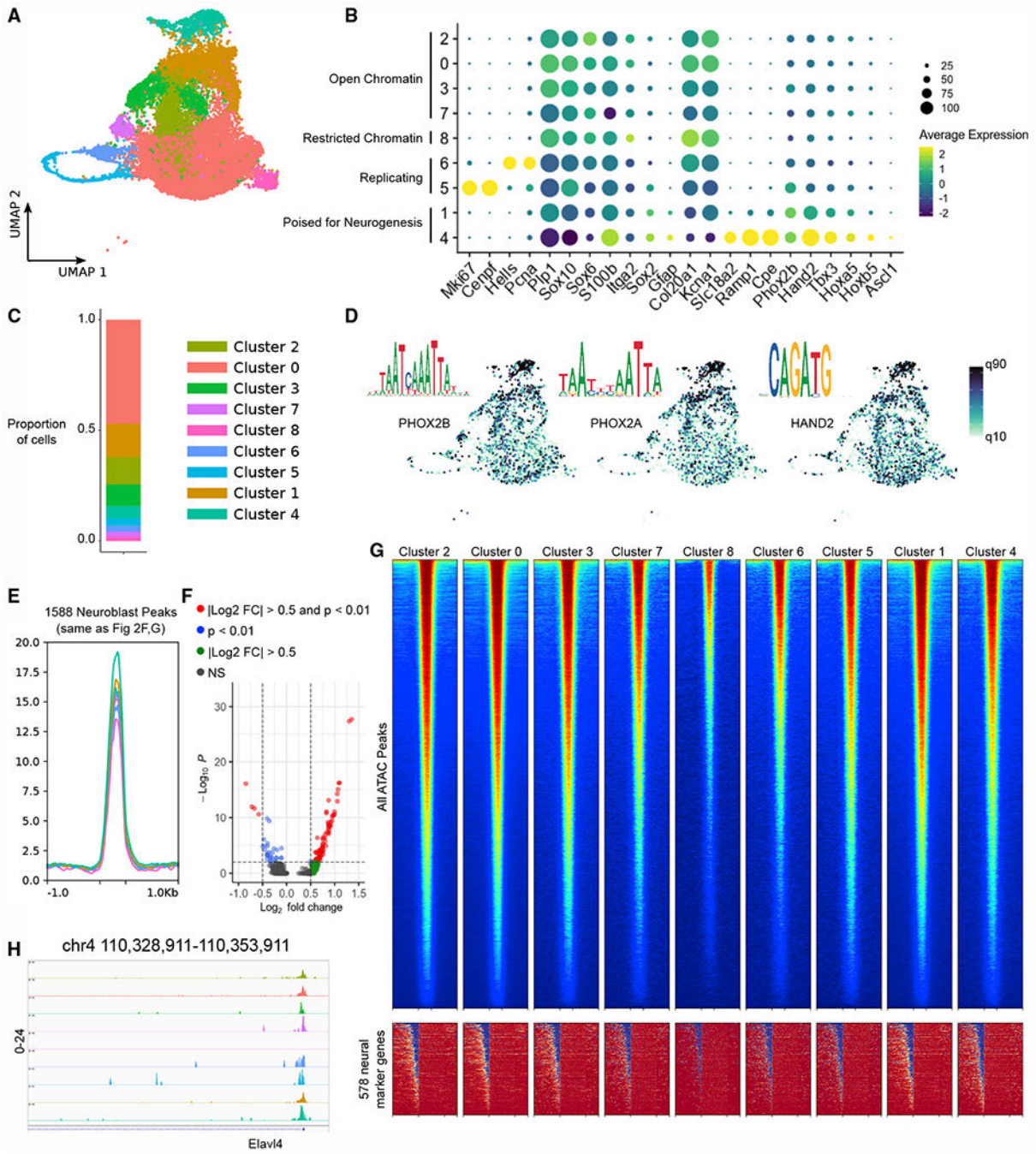

Figure 3. Small intestinal myenteric glia are transcriptionally diverse and contain cells poised for neurogenesis

(A) UMAP of 17,690 GFP+ cells sorted from the small intestine of *Pip1::GFP* mice near P14, with dimensional reduction performed based on differential gene expression.

(B) Dot plot showing expression of selected genes within cluster. Dot size indicates the percentage of cells in each cluster with >0 transcripts detected, while color indicates the relative level of gene expression. Cluster arrangement on the y axis is based on hierarchical clustering using expression of the displayed genes. Clusters are annotated to the left based

Author Manuscript Author Manuscript Author Manuscript Author Manuscript

on gene expression, chromatin accessibility at neuronal marker peaks, and motif enrichment patterns.

(C) Proportion of cells contained within each cluster.

(D) UMAPs colored based on enrichment for the indicated transcription factor binding motifs, with cutoffs at the 10^{th} and 90^{th} quantiles. Also shown are position frequency plots for the indicated motifs.

(E) Profile plots showing average signal intensity at the indicated set of peaks. Peaks are scaled to 500 bps, and 1,000 bps up- and downstream are shown.

(F) Volcano plot showing adjusted p values and log2 fold ATAC signal of 457 neuroblast-associated peaks with >0 counts in both cluster 4 and all other clusters. Points farther to the right on the x axis indicate increased signal in cluster 4, while points to the left indicate increased signal in all other clusters.

(G) Heatmaps showing ATAC signal within each cluster at all 94,210 ATAC peaks identified in the dataset by MACS2 (top) and around the gene body of 578 marker genes for neuroblasts and neurons identified within the dataset (bottom). ATAC peaks (top) are scaled to 500 bps, and 1,000 bps up- and downstream are shown, while gene bodies (bottom) are scaled to 2,000 bps, and 2,000 bps upstream and 1,000 bps downstream are shown.

(H) GV Browser track showing ATAC signal within each cluster in the region around the *Elavl4* TSS.

Author Manuscript Author Manuscript Author Manuscript Author Manuscript

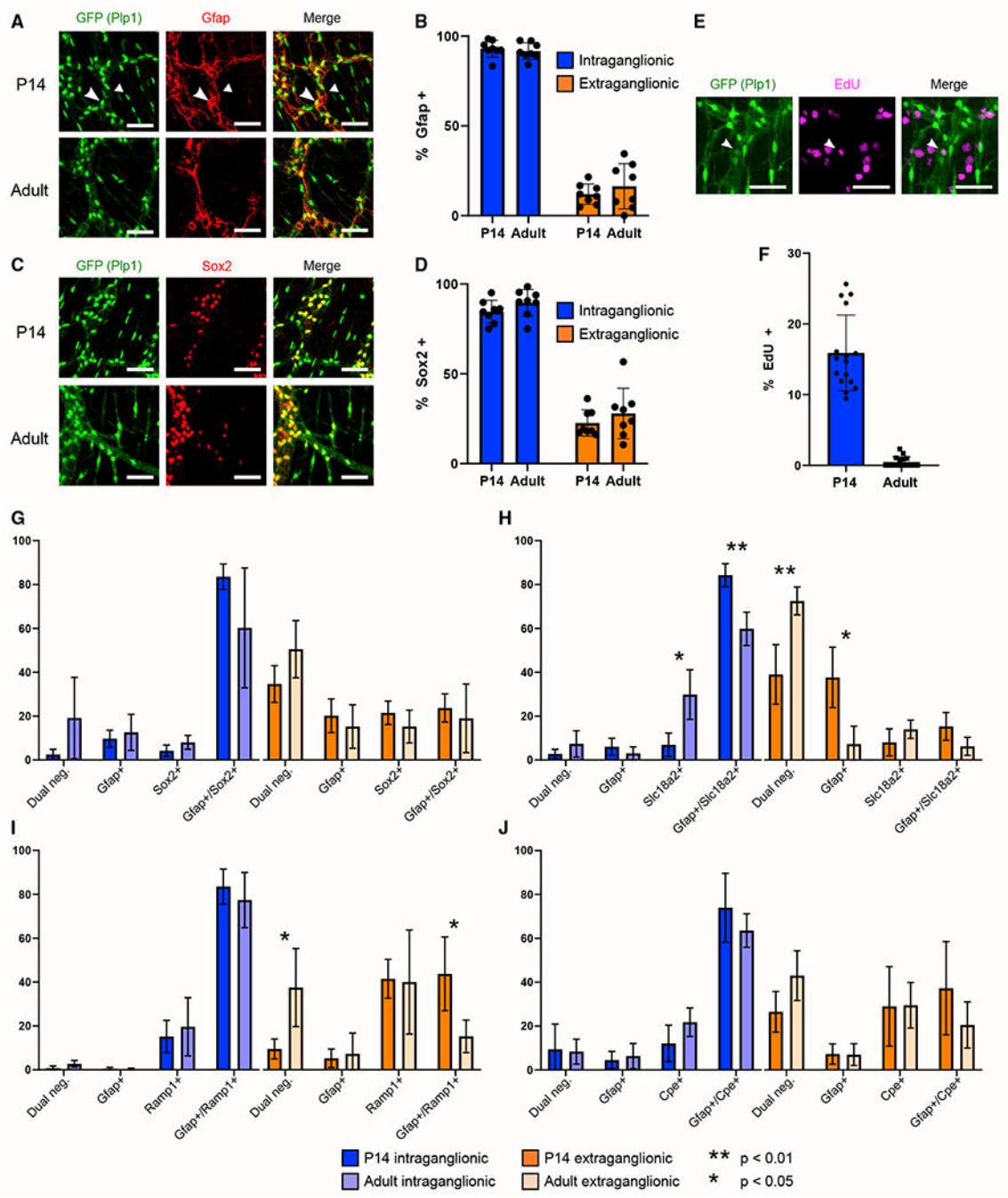

Figure 4. IF and RNAscope confirm intraganglionic EGCs are enriched with cells poised for neurogenesis in both the early postnatal period and after weaning

(A and C) Representative confocal microscopy images of IF staining of EGCs in the LMMP of *Plp1::GFP* mice of the indicated ages, with staining for Gfap (A) or Sox2 (C). Examples of intraganglionic (large arrowhead) and extraganglionic (small arrowhead) EGCs are indicated on the top row. Scale bar indicates 50 μm.

(B and D) Quantification of IF staining shown in (A) and (C). Error bars represent standard deviation. Data within each age group represent quantification of 4 images each from 2 mice.

Author Manuscript Author Manuscript Author Manuscript Author Manuscript

(E) Example confocal microscopy image showing an intraganglionic EGC from a postweaning mouse (age 14 weeks) that incorporated EdU, indicating proliferation. Arrowhead shown to highlight the EGC with EdU incorporation. Scale bar indicates 50 μm.

(F) Quantification of EdU+ intraganglionic EGCs in P14 mice and postweaning mice (age 14 weeks). Error bars represent standard deviation. Data within each age group represent quantification of 8 images each from 2 mice.

(G–J) Quantification of the proportion of intra- and extraganglionic EGCs with RNAscope signal for the indicated combinations of transcripts in either P14 mice or postweaning animals (age 14 weeks). n = 4 for each sample, with 2 tiled sections of LMMP tissue analyzed in each of 2 mice. Error bars represent standard deviation, and p values were calculated using a two-sided unpaired Student's t test.

Author Manuscript Author Manuscript Author Manuscript Author Manuscript

KEY RESOURCES TABLE

REAGENT or RESOURCE	SOURCE	IDENTIFIER
Antibodies		
Anti-GFP	Abcam	ab13970; RRID: AB_300798
Anti-Gfap	Abcam	Ab53554; RRID: AB_880202
Anti-Sox2	R&D Systems	AF2018; RRID: AB_355110
Donkey anti-Goat IgG (H + L) Cross-Adsorbed Secondary Antibody, Alexa Fluor 546	Invitrogen	A-11056; RRID: AB_2534103
Goat anti-Chicken IgY (H + L) Secondary Antibody, Alexa Fluor 647	Invitrogen	A-21449; RRID: AB_2535866
Chemicals, peptides, and recombinant proteins		
EdU (5-ethynyl-2′-deoxyuridine)	Invitrogen	A10044
DAPI (4′,6-Diamidino-2-Phenylindole, Dihydrochloride)	Invitrogen	D1306
RNAscope Probe Mm-Gfap-C3	ACD	313211-C3
RNAscope Probe Mm-Sox2-C2	ACD	401041-C2
RNAscope Probe Mm-Slc18a2	ACD	425331
RNAscope Probe Mm-Ramp1-C2	ACD	532681-C2
RNAscope Probe Mm-Cpe	ACD	454091
Critical commercial assays		
Click-iT EdU Cell Proliferation Kit for Imaging, Alexa Fluor 647 dye	Fisher Scientific	C10340
RNA-Protein Co-detection Ancillary Kit	ACD	323180
RNAscope Multiplex Fluorescent Reagent Kit v2	ACD	323100
Deposited data		
Raw and analyzed single-cell sequencing data	This paper	GEO: GSE184981
Raw RNAscope data	This paper	https://doi.org/10.17632/kjd9vn9r3p.1
Raw immunoflouresence data	This paper	https://doi.org/10.17632/jjyt27z4sp.1
Raw microscopy data for differentiation of enteric glial cells in culture	This paper	https://doi.org/10.17632/g2rv2g468f.2
Raw microscopy data for emergence of enteric neurons in neurosphere cultures	This paper	https://doi.org/10.17632/c4kj42g9p2.1
Experimental models: Organisms/strains		
Mouse: Plp1::GFP	Mallon et al., 2002; The Jackson Laboratory	JAX: 033357
Mouse: Actl6b::Cre	The Jackson Laboratory	JAX: 027826
Mouse: (R)26-tdTomato	The Jackson Laboratory	JAX: 007914
Software and algorithms		
Cell Ranger	(Zheng et al.)[49]	https://support.10xgenomics.com/single-cell-gene-expression/software/overview/welcome
Seurat	Satija Lab	https://satijalab.org/seurat/
Signac	Stuart Lab	https://stuartlab.org/signac/
MACS2	(Zhang et al.)[50]	https://pypi.org/project/MACS2/

Author Manuscript

Author Manuscript

Author Manuscript

Author Manuscript

REAGENT or RESOURCE	SOURCE	IDENTIFIER
ChromVAR	(Schep et al.)[26]	https://greenleaflab.github.io/chromVAR/index.html
Sinto	Tim Stuart, Satija Lab	https://timoast.github.io/sinto/
deepTools	(Ramírez et al.)[51]	https://deeptools.readthedocs.io/en/develop/index.html
Integrative Genomics Viewer	The IGV Team	https://igv.org/
LAS X	Leica	https://www.leica-microsystems.com/products/microscope-software/p/leica-las-x-ls/
Prism	GraphPad Software	https://www.graphpad.com/scientific-software/prism/
ImageJ	National Institutes of Health	https://imagej.nih.gov/ij/